Continuum simulation of the discharge of the granular silo

L. Staron, P.-Y. Lagrée and S. Popinet

Regular Article

Continuum simulation of the discharge of the granular silo

A validation test for the $\mu(I)$ visco-plastic flow law

L. Staron[1,2,a], P.-Y. Lagrée[2], and S. Popinet[2,3]

[1] School of Earth Sciences, University of Bristol, Queens Road, Bristol BR8 1RJ, United Kingdom
[2] CNRS - Université Pierre et Marie Curie Paris 6, UMR 7190, Institut Jean Le Rond d'Alembert, F-75005 Paris, France
[3] National Institute of Water and Atmospheric Research, PO Box 14-901 Kilbirnie, Wellington, New Zealand

Abstract. Using a continuum Navier-Stokes solver with the $\mu(I)$ flow law implemented to model the viscous behavior, and the discrete Contact Dynamics algorithm, the discharge of granular silos is simulated in two dimensions from the early stages of the discharge until complete release of the material. In both cases, the Beverloo scaling is recovered. We first do not attempt a quantitative comparison, but focus on the qualitative behavior of velocity and pressure at different locations in the flow. A good agreement for the velocity is obtained in the regions of rapid flows, while areas of slow creep are not entirely captured by the continuum model. The pressure field shows a general good agreement, while bulk deformations are found to be similar in both approaches. The influence of the parameters of the $\mu(I)$ flow law is systematically investigated, showing the importance of the dependence on the inertial number I to achieve quantitative agreement between continuum and discrete discharge. However, potential problems involving the systems size, the configuration and "non-local" effects, are suggested. Yet the general ability of the continuum model to reproduce qualitatively the granular behavior is found to be very encouraging.

1 Introduction

Granular matter is a well-known example of complex material able to flow like a viscous fluid or resist shear stress like a solid, and evolving from one state to the other over a distance of typically few grain diameters. During the discharge of a silo, this property is responsible for the co-existence of rapid dilute flow in the vicinity of the outlet, dense slower shear in the higher parts of the bulk, and static regions at the bottom of the container. In some instances, when the outlet can accommodate only few particles diameters, arching —the formation of highly loaded force chains— occurs above the orifice, whereby flow is stopped, or made intermittent [1,2].

Silos are widely used in geo-technical or agro-technical applications, for which the full understanding of the discharge dynamics and its reliable modeling are critical [3,4]. Meanwhile, the variety of behaviors exhibited in a silo justifies the large academic interest granted to the subject. As a result, much understanding has been gained on the silo phenomenology, from "why hour glasses tick", to the Beverloo scaling for the discharge rate or the shape of the free surface [5–8]. Because of the specificity of its behavior, the granular silo is a stringent test for continuum modeling of granular matter [9–12]. The fact that the silo outlet may be of a little number of grains size, hence

threatening the validity of a continuous approach, forms a first complication: indeed, uninterrupted flows may be obtained for outlet size as small as 5 grain diameters [13]. While the modeling of the intermittent flow regime is hardly accessible to continuum modeling, it is not clear that well-developed flows over such small length-scales are well captured either [14]. The main difficulty however is the existence of static and rapidly flowing zones simultaneously. This requires a unified picture of what is often described as solid-like and fluid-like behaviors, each of them forming a challenge of its own. The solid-like behavior of granular matter is characterized by the small domain of elastic response, a plastic threshold whose dependence on the grains properties and packing history is unclear, and important force fluctuations which may compromise the validity of a continuum picture at the scale of few grain diameters [15,16]. The fluid-like behavior also has its share of difficulty, and offers a wide variety of complicated behaviors depending on the system geometry. They have recently benefited from important progress with the formulation of the $\mu(I)$ flow law [17–19]. Achieving a continuum picture of a system as complete as the granular silos requires a reliable physical modeling of both fluid-like and solid-like properties. This may be undertaken either by generalizing elasto-plastic approaches to rapidly moving zone [9,20], or by considering the system as a viscous flow with areas of infinite viscosity [11,21]. The first ap-

[a] e-mail: lydie.staron@upmc.fr, staron@lmm.jussieu.fr

proach was applied in [10] to the initial stages of the silo discharge, where stress and velocity fields were found to match those observed in DEM simulations. Therefore, the plastic part of the deformations (namely developed flow) was chosen to obey the $\mu(I)$ flow law. In this contribution, we adopt the fluid approach, namely we approximate the granular matter as a viscous material flowing following fluid mechanics equations. As in [11,19,21], and following the choice of [10], we adopt the $\mu(I)$ flow law to describe the viscous behavior of the granular matter [17]. Doing so, we are able to simulate in two dimensions all the stages of the silo discharge, from the onset to the complete release of the material. Comparison with discrete simulations of granular silos are carried out. In both cases, the Beverloo scaling is recovered. Adjusting rheological parameters to make discrete and continuum discharge coinciding being non-trivial, we do not attempt a quantitative comparison first, but focus on the qualitative behavior of velocity and pressure at different locations in the flow. A good agreement is obtained in the regions of rapid flows, while areas of slow creep are not entirely captured by the continuum model. The pressure field shows a general good agreement, and bulk deformations in the two approaches are found to be very similar. The influence of the parameters of the $\mu(I)$ flow law is systematically investigated, showing the importance of the dependence on the inertial number I to achieve quantitative agreement between continuum and discrete discharge, and allowing discussion on the limitations of the model. Finally, the effect of the spatial mesh refinement and the effect of the boundary conditions in the case of the continuum model are studied and found to be weak.

2 Modeling discrete and continuum granular silos

2.1 A continuum model for granular flows

Defining mean viscous properties for granular flows that would be able to describe the sharp transition between rapid flow, creep motion and quasi-static state (observed for instance in the silo configuration, in avalanches on erodible beds, and in all transient flows) has proven a long-lasting obstacle to efficient modeling of granular flows. The most obvious difficulty is to characterize the divergence of the viscosity, or jamming transition. A strategy to bypass this difficulty is to forego the explicit definition of the viscosity and to rely instead on the frictional properties of granular matter which relate pressure and shear stress: $\tau = \mu P$, where μ is the effective friction of the material and P the pressure. Assuming that shear rate and shear deformation are collinear (which is the case in simple flow configuration like chute flows, but less obvious in more complex configuration like silos of collapsing columns [21,22]), a relation can be derived between shear rate and shear stress which can be used as a substitute for viscosity:

$$\boldsymbol{\tau} = \frac{\mu P}{\|\dot{\gamma}\|}\dot{\gamma}, \tag{1}$$

where $\dot{\gamma}$ and $\|\dot{\gamma}\|$ are the shear rate and the norm of the shear rate, respectively. This strategy was first successfully applied for a simple flow configuration, and later in more complex configurations, including the silo [10,11,19,21,23]. This strategy is also adopted in this work.

According to relation (1), a constant friction model ($\mu = $ cst), as simple as it is, will nevertheless lead to a non-trivial viscous behavior, showing shear-thinning properties and a dependence on the local pressure. This case is addressed in section 6.1. In this contribution however, we are interested is assessing the performances of the $\mu(I)$ flow law. Established on the basis of experimental and numerical works in various simple flow configurations (planar shear, couette flow, chute flows and rotating drums (see [17] and references therein)), it has since led to the successful recovery of granular dynamics in more testing situations: 3D chute flow with rough side walls [19], the early stage of the discharge of a granular silo [10], or the collapse of granular columns under gravity [21] for instance.

The $\mu(I)$ flow law implemented in this work is identical to that used in [19]: μ is a function of the non-dimensional number $I = d\|\dot{\gamma}\|/\sqrt{P/\rho}$, where d is the mean grain diameter and ρ the density, following the dependence

$$\mu = \mu_s + \frac{\Delta\mu}{1 + I_0/I}, \tag{2}$$

where μ_s, $\Delta\mu$ and I_0 are constants [19]. Based on previous work comparing the rapid flow of discrete granular systems and their continuum counterpart in the column collapse configuration [21], we first chose $\mu_s = 0.32$, $\Delta\mu = 0.28$ and $I_0 = 0.4$. The influence of the value of these parameters is specifically addressed in sect. 6.1.

The dependence of the friction properties on the non-dimensional number I (whose relevance to granular flows was also discussed in [24]) conveys the fact that the local dynamics of the grains rearranging under a given pressure when submitted to a given macroscopic deformation reflects in the dissipation properties. It describes a dependence on the dynamics, according to which the frictional properties of the flow vary between two extremal values: a smaller one corresponding to static state and a larger one corresponding to rapid flow. The precise shape of the dependence itself, as observed in experiments and simulations, may be questioned: in [25] for instance, a power-law dependence is proposed. In this contribution, the sensitivity of the results to the shape of the increase of μ with I (eq. (2)) is not investigated. Rather, we discuss in detail the implication of the dependence, and its role in the ability of the continuum model to reproduce the outcome of discrete simulations (sect. 6.1).

More elaborate rheological models may account for non-local effects [26,27] or incorporate explicitly the granular micro-structure [28]. These aspects are not included in the present discussion. We will see however that, in spite of its simplicity, the $\mu(I)$ flow law leads to the recovery of a large part of the granular silo phenomenology, which we reproduce using discrete numerical simulations.
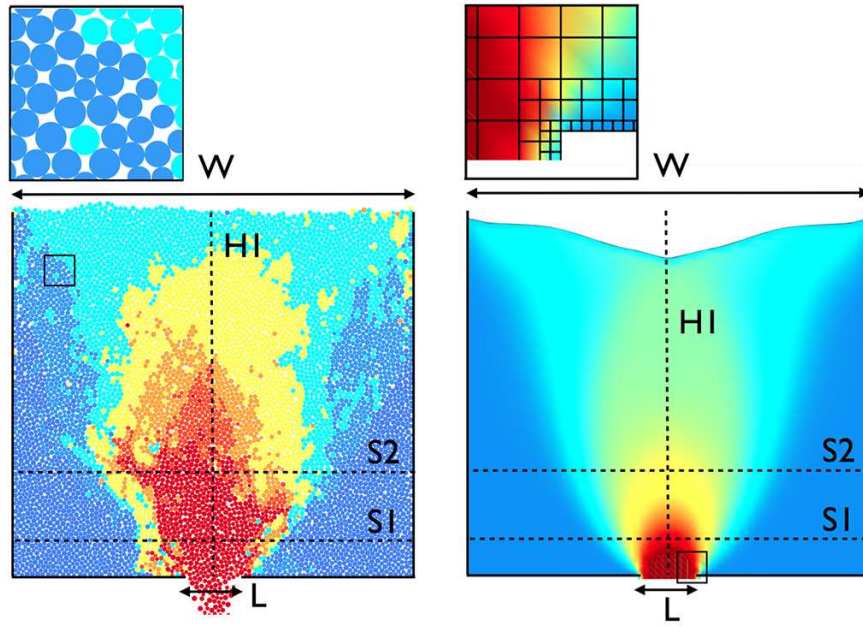
Fig. 1. (Color online) Discrete silo simulated by Contact Dynamics (left) and continuum silo simulated by Gerris (right); the outlet size is L, the silo width is W; S_1, S_2 and H_1 are cross-sections along which velocity and pressure are analyzed.

2.2 The visco-plastic silo using a Navier-Stokes solver

The continuum simulations were performed using the Gerris flow solver in two dimensions, which solves the Navier-Stokes equation for a bi-phasic mixture applying a Volume-Of-Fluid approach [29,30]. The existence of two fluids translates numerically in different viscosity and density on the simulation grid following the advection of the volume fraction representing the proportion of each fluid. In our case, one fluid stands for granular matter (characterized by the coefficient of internal friction μ) and the other stands for the surrounding air. In [21], we established that the dynamics of a rapid granular layer is not affected by the surrounding fluid if the latter has a density and viscosity small enough relatively to those of the granular layer; accordingly, we chose a ratio of 10^{-2} between the density and viscosity of the two fluids. The position of the interface between the two fluids is solved in the course of time based on the spatial distribution of their volume fraction. The Navier-Stokes equations

$$\boldsymbol{\nabla} \cdot \boldsymbol{u} = 0,$$
$$\rho \left(\frac{\partial \boldsymbol{u}}{\partial t} + \boldsymbol{u} \cdot \boldsymbol{\nabla} \boldsymbol{u} \right) = -\boldsymbol{\nabla} p + \boldsymbol{\nabla} \cdot (2\boldsymbol{\eta} \boldsymbol{D}) + \rho \boldsymbol{g}$$

are thus solved for a two-phase flow, namely granular matter and air, with a variable fraction function c

$$\frac{\partial c}{\partial t} + \boldsymbol{\nabla} \cdot (c\boldsymbol{u}) = 0,$$
$$\rho = c\,\rho_{\text{grains}} + (1-c)\rho_{\text{air}},$$
$$\eta = c\,\eta_{\text{grains}} + (1-c)\eta_{\text{air}}.$$

As explained in subsect. 2.1 (relation (1)), the viscosity η_{grains} of the granular matter is approximated by mean of the friction properties [19,23]

$$\eta_{\text{grains}} = \min\left(\frac{\mu(I)P}{D_2}, \eta_{\text{max}} \right), \qquad (3)$$

where μ is the effective coefficient of friction of the granular flow, P is the local pressure and D_2 is the second invariant of the strain rate tensor $\boldsymbol{D}$: $D_2 = \sqrt{D_{ij}D_{ij}}$. For large values of D_2, the viscosity is finite and proportional to μ and P; when D_2 reaches low values, the viscosity η diverges. Numerically, this divergence is bounded by a maximum value η_{max} chosen to be 10^4 times the minimum value of η; we have checked that the choice of η_{max} did not affect the results as long as η_{max} is large enough (at least 10^2 times the minimum value of η).

2.3 The discrete silo using Contact Dynamics

The discrete simulations are performed using the Contact Dynamics algorithm [31,32]. The grains are perfectly rigid and obey a strict non-overlap condition at contact. They interact through a Coulombic friction law, imposing that the tangential force at contact f_t is related to the normal force at the same contact f_n through the inequality $|f_t| \leq \mu_c f_n$, where μ_c is the coefficient of friction at contact. A coefficient of restitution e prescribes the amount of energy dissipated during collisions. In a given configuration, the algorithm finds all the forces compatible with the constraints, geometrical and frictional, imposed at each contact. This method has proven a reliable tool to reproduce the behavior of granular matter in many configurations. Further details on the numerical method can be found in [31–33].
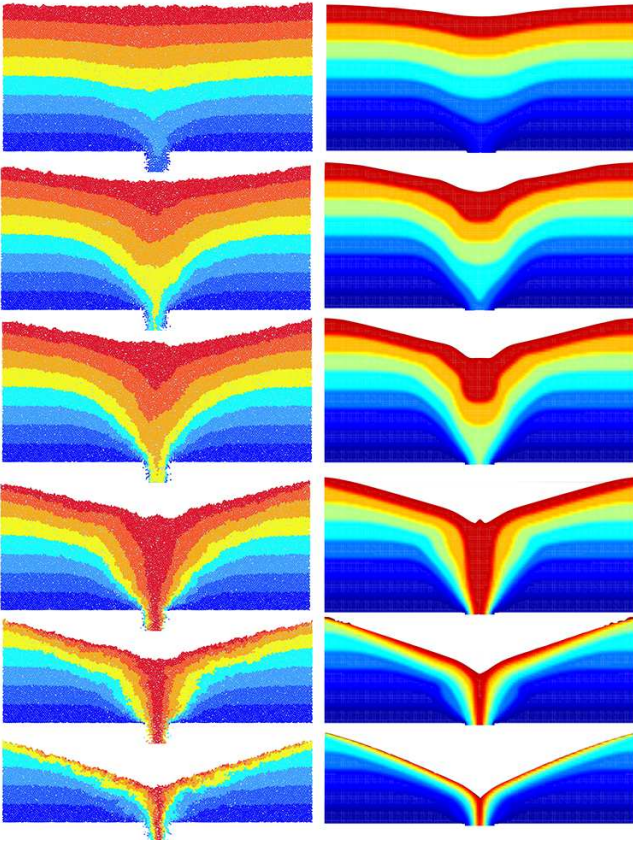
Fig. 2. (Color online) Inner deformations in granular discrete (left) and continuum (right) silos with $W = 180d$, and $L = 16.9d$, for $\bar{t} = t/T_0 = 0.06, 0.12, 0.17, 0.26, 0.56$ and 0.62, where T_0 is the duration of the discharge. The different colors are used as tracers.

The simulations discussed in this contribution are performed with a value of the coefficient of restitution set to $e = 0.5$, which favor dense flow regimes. The value of the coefficient of friction is set to $\mu_c = 0.5$ (glass beads have a coefficient of friction of about 0.2, and sand grains have a coefficient of friction that may vary a lot, but 0.5 is consistent). The influence of these two parameters on the flow characteristics was not investigated. Instead, we focus on the silo's geometrical characteristics to allow comparison with the continuum simulations.

2.4 Flow configuration

The flow configuration investigated, using both continuum or discrete approaches, is a two-dimensional flat-bottomed silo, of width W, initial filling height H and outlet L (see fig. 1). The width of the silo is $W = 90d$ or $W = 180d$; this corresponds to 8066 and 16240 discrete grains, respectively. The initial filling height is $H = 90d$, and was not varied. The grains show a slight size dispersity to avoid ordering effect. In the case of discrete simulations, the walls of the silo are smooth, and contacts between grains and walls show the same properties (*i.e.* same coefficients e and
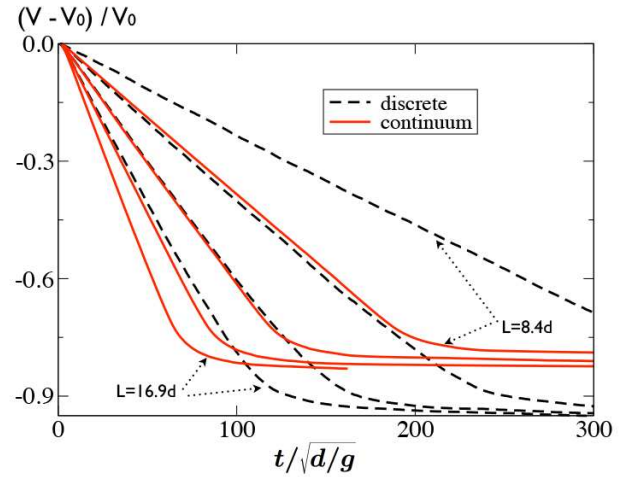

Fig. 3. Normalized volume of granular matter left in the silo as a function of the normalized time $t/\sqrt{d/g}$ for discrete (dashed line) and continuum (solid line) simulations, for outlet $L/d = 8.4, 11.2, 14.1$ and 16.9.

μ_c) as contacts between grains. For the continuum silo, a zero-pressure condition is imposed at the top boundary and at the outlet. A no-slip boundary condition is imposed at the side walls and at the bottom wall; the effect of this choice compared to free-slip condition is discussed in sect. 7.

Considering geometrically perfectly identical continuum and discrete granular silos, we can now compare their respective behavior during discharge. Figure 2 shows the inner deformations occurring during the discharge at different moments using colors to trace down the particles (either grains or fluid volumes). The general agreement between the two is good. Note that the singularity observed above the outlet in the continuum case for $t/T_0 = 0.26$ was observed experimentally in [8], and is also visible in discrete simulations in the shape of a little mounded swell.

3 The discharge rate

Granular silos have the well-known particularity of releasing their stored material at a constant rate. The discharge process, as a consequence, is independent of the height of material left in the silo, and thus, seems independent of the mean pressure inside the silo itself. This particularity is captured by the Berverloo scaling [5], which relates the discharge rate Q to the silo outlet L according to the following scaling, provided L is large enough [13, 34]

$$Q = C\sqrt{g}(L - kd)^{N-1/2}, \qquad (4)$$

where N is the dimension of the problem, and C and k are non-dimensional constants. The constant k is classically interpreted as a volume of exclusion due to steric constraints applied by the rigid grains, reducing the effective size of the outlet $(L - kd)^{N-1}$ by a multiple of the grain diameter d; a typical value for k is 2 (in the original paper for instance, Beverloo and co-authors find $k = 2.9$
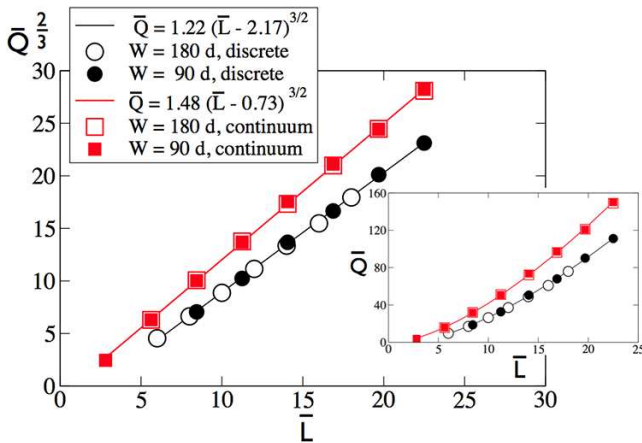
Fig. 4. Normalized discharge rate $\bar{Q} = Q/\sqrt{g}d^{3/2}$ as a function of the normalized outlet size $\bar{L} = L/d$ for silos width $W = 90d$ and $W = 180d$, for discrete and continuum simulation with corresponding Beverloo scalings in solid lines (see eq. (4)).

for sand and $k = 1.3$ for watercress seeds in an axisymmetric setting). The constant k can also be seen as reflecting the discharge velocity through the term $\sqrt{g}(L - kd)^{1/2}$, following variations induced by the viscous properties of the flow and the shape of the velocity profile at the outlet [35]. The constant C is typically of 0.5 in 3D [5].

Although the range of validity of the Beverloo scaling is bounded, small and very large apertures inducing different behaviors [13], it is surprisingly robust, and was recovered both numerically and experimentally for a great variety of granular matter [36–42].

The physical origin of this scaling is often attributed to the Janssen effect: a pressure screening created by the mobilization of friction forces at the walls prevents the lower region of the silo to "sense" the pressure state [3,43–46]. In contradiction to this explanation, experimental works have shown that the Beverloo scaling holds in configurations where Janssen effect could not be active [39,40]. Recently, continuum simulations of the silo discharge using the continuum approach applied in this paper suggest that the Beverloo scaling results from the yield stress properties of the material [11], in agreement with [47]. This aspect, still debated, will not be discussed here. Instead, we compare the discharge of the discrete granular silos simulated by contacts dynamics and the discharge of continuum granular silos simulated by the solver Gerris with the $\mu(I)$ flow law, and focus on the consistency between the two approaches.

3.1 Recovering the Beverloo scaling

In a first set of simulations, we perform series of silo discharges with $W = 90d$, and with outlet size L exactly similar in the discrete and the continuum cases, in order to allow direct comparison. We consider L varying from $L = 5.63d$ to $L = 22.5d$. The evolution of the volume V left in the silo (normalized by the initial volume V_0) is reported in fig. 3 as a function of time
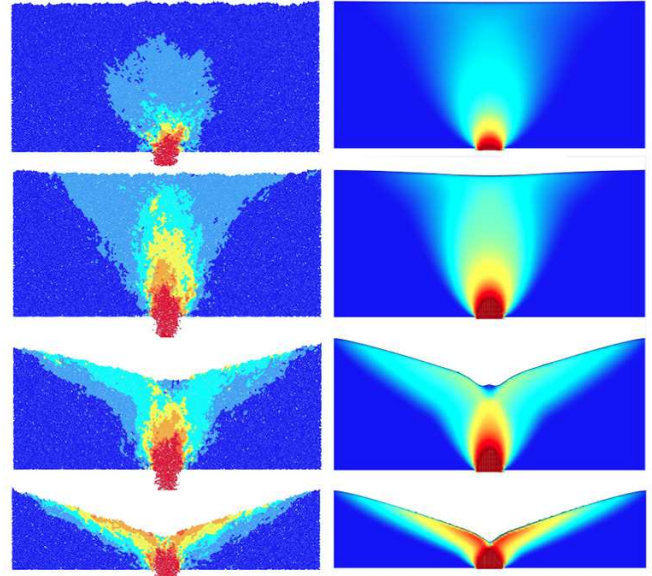

Fig. 5. (Color online) Velocity field for discrete simulation and continuum simulation with $L = 16.8d$ throughout the discharge process. The color scale is linear, with an upper-bound value shown in red color.

(normalized by $\sqrt{d/g}$). For both discrete and continuum cases, the discharge rate is constant, in agreement with experimental observation. The normalized discharge rate $\bar{Q} = Q/\sqrt{g}d^{3/2}$ can thus be plotted as a function of $\bar{L} = L/d$. For both discrete and continuum silos, we recover the Berverloo scaling (fig. 4)

$$Q = 1.22\sqrt{g}(L - 2.17d)^{3/2} \text{ for discrete,} \tag{5}$$

$$Q = 1.48\sqrt{g}(L - 0.73d)^{3/2} \text{ for continuum.} \tag{6}$$

The Beverloo scaling was recovered in many instances using discrete simulations [36,38,41,48–50], showing the robustness of this flow behavior. Observing this typical granular phenomenology in the case of the discharge of a viscous flow, though non-Newtonian, is however not trivial [11].

No prior adjustment of the rheological parameters was made: we use $\mu_s = 0.32$, $\Delta\mu = 0.28$ and $I_0 = 0.4$ for the continuum simulations, $\mu_c = 0.5$ and $e = 0.5$ for the discrete simulations. Hence we do not expect the two approaches to coincide quantitatively at this stage. Nevertheless, beside the fact that the continuum discharge is more rapid for a given L (corresponding to a large prefactor C), two important differences can be noted. Expectedly, the grains rigidity in the discrete case leads to a lower effective outlet $(L - kd)$: $k = 2.17$ for discrete simulations, while $k = 0.73$ for continuum (see scalings (5) and (6)). Moreover, for a given outlet size L, the discrete discharge is more efficient: $\simeq 95\%$ of material evacuated, against $\simeq 80\%$ for the continuum discharge.
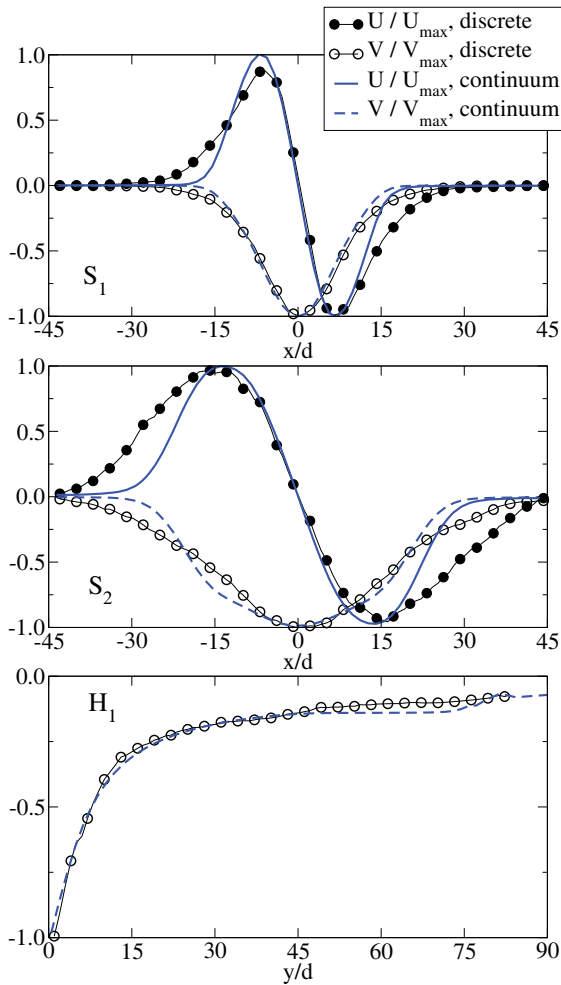
Fig. 6. Horizontal and vertical velocity profiles for granular and continuum silos along cross-sections S_1 and S_2, and vertical axis H_1, rescaled by the velocities maximum values, for $L = 11.2d$. (See fig. 1 for localization of sections S_1 and S_2 and H_1.)

3.2 Influence of the silo's width

To check the influence of the silo's width W (mobilization of friction forces at the walls being often resorted to as explanation for the Beverloo scaling), we perform series of simulations with larger silos with $W = 180d$ instead of $W = 90d$. As previously, for both discrete and continuum simulations, we plot the normalized discharge rate $\bar{Q}$ as a function of the normalized outlet size $\bar{L}$ in fig. 4 for $W = 180d$, together with the results obtained for $W = 90d$. We observe that the value of W, at least in the range considered here, has no effect on the discharge rate. This result tends to show that the discharge is dominated by local factors, rather than by the state of the system at the walls.

The influence of the initial height of material stored in the silo was not investigated here. While we expect the latter to have no influence on the silo discharge in the case of discrete simulations, this is not obvious in the case of continuum simulations. This aspect was studied in detail

in [11], showing that the influence of initial height in the continuum silo discharge is weak.

4 The velocity field

From the shape of the Beverloo scaling, and according to intuition, it seems expected that the discharge velocity and the velocity field in the bulk of the silo will depend on the value of the rheological parameters adopted. At this stage, no prior adjustment was performed to make the continuum and discrete discharge coinciding quantitatively (this non-trivial aspect being discussed in details in sect. 6.1); hence, quantitative comparison of the velocity field for the two approaches is not possible straightaway. However, qualitative comparison of the shape of the velocity field for different apertures and along different profiles is possible.

For visual inspection, fig. 5 shows snapshots of the velocity field during the discharge of a discrete and a continuum silo with $W = 180d$ and $L = 16.9d$, at different instants, and using the same color scale. We observe a reasonable agreement, with the areas of slow shear developing from the sides of the outlet to the bulk and the free surface, and the area of rapid flow being confined above the outlet.

Figure 6 shows the horizontal and vertical velocities profiles along the cross-sections S_1 and S_2, as well as along the vertical axis H_1 (see fig. 1 for locating S_1, S_2 and H_1), for an outlet size $L = 11.2d$, at $T = 10\sqrt{d/g}$ and after normalization of the horizontal and vertical velocities by their maximum values $U_{\max}$ and $V_{\max}$, respectively. The shape of the horizontal profiles S_1 and S_2 reproduces the shape already observed elsewhere numerically and experimentally [14,37,51]. Continuum and discrete models show a reasonable qualitative agreement right above the outlet (profiles along S_1), but tend to differ in the area of the outlet edges, where the velocity decreases towards zero, and higher in the bulk (profiles along S_2). The transition from a flowing state to a static one is sharper in the continuum systems, while discrete systems exhibit a larger area of slow shear before freezing in a static state. Yet, the area of rapid flow is well reproduced by the continuum model. Figure 7 shows the velocity profiles along the cross-section S_1 for three other cases $L = 8.4d$, $L = 14.1d$ and $L = 19.7d$. The same conclusions apply: the shape of the rapid flow is well captured by the continuum model, but areas of slower motion tend to differ.

5 The pressure field

Maps of the pressure field are shown in fig. 8 at different instants of the discharge for both discrete and continuum systems. In the discrete case, the pressure is averaged over squares of 7 grains diameters sides. The following features are visible for both approaches: a lower pressure above the outlet, and a maximum of pressure aside the outlet.

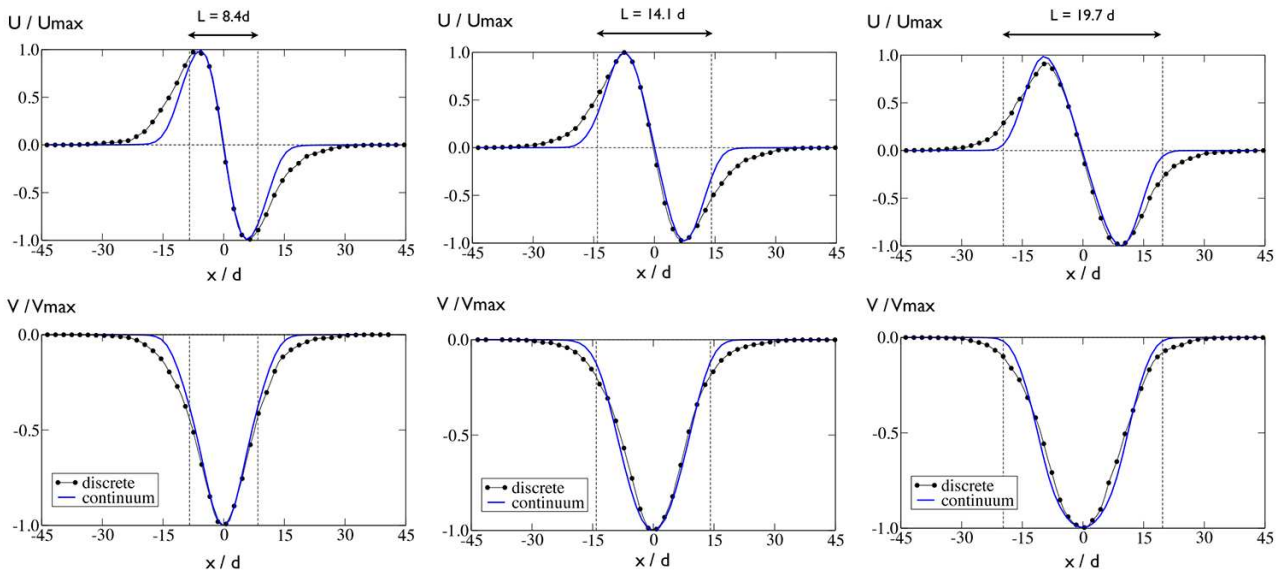The pressure field in a silo is known to obey a nontrivial distribution due to the presence of confining walls

Fig. 7. Horizontal (U) and vertical (V) velocity profiles along the cross-section S_1, normalized by their maximum values $U_{\max}$ and $V_{\max}$, respectively, for granular and continuum silos with outlet size $L = 8.4d$ (left), $L = 14.1d$ (middle) and $L = 19.7d$ (right).
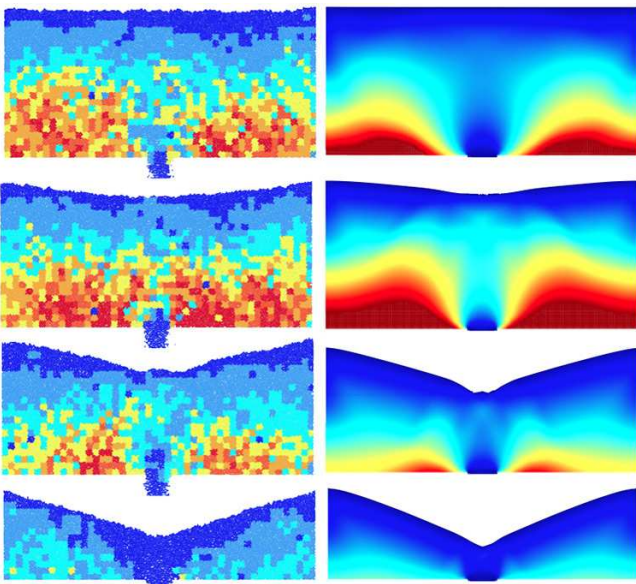

Fig. 8. (Color online) Pressure field for discrete and continuum simulations with $L = 16.8d$ throughout the discharge process. The color scale is linear, with an upper-bound value of $0.78\rho gH$ (in red).

and the existence of a low-pressure condition created by the outlet [43, 46]. Another factor affecting the pressure field are the yield stress properties of the material [11] (this is further illustrated in sect. 6.1); as a consequence, quantitative comparison of the pressure field in discrete and continuum silos is not readily possible without adjusting the rheological parameters. However, a qualitative comparison of pressure profiles can be performed. In fig. 9, pressure profiles along the cross-sections S_1, S_2 and vertical axis H_1 are shown for silos of outlet $L = 11.2d$, at

$T = 10\sqrt{d/g}$, and for the rheological parameters considered so far (*i.e.* $\mu_s = 0.32$, $\Delta\mu = 0.28$ and $I_0 = 0.4$ for the continuum simulations, $\mu_c = 0.5$ and $e = 0.5$ for the discrete simulations). The result for discrete simulations is averaged over a larger time-window in order to reduce (but not supress) the large fluctuations characteristic for granular matter. These fluctuations are much higher in the static zone (closer to the walls), where force chains can form through enduring contacts; areas of rapid flow (closer to the outlet) where contacts are short-lived, are much smoother. The pressure field exhibits strong variations at a given height, with a marked minimum above the outlet even at a significant distance away from it (as along section S_2). Discrete and continuum simulations share the following features: a marked dip of pressure above the outlet, the existence of two high-pressure regions on one and the other side of the outlet, and a slighter decrease close to the walls. This coarse but general agreement in the shape of the profiles endures for different values of L.

6 More on the Beverloo scaling

So far, no attempt was made to maximize the agreement between continuum and discrete approaches in terms of their discharge, that is, in terms of the Beverloo scaling. Adjusting appropriately the various rheological parameters is expected to lead to quantitative agreement between both. We recall the shape of the friction law adopted to approximate the continuum viscous behaviour: $\mu = \mu_s + \Delta\mu/(1 + I_0/I)$, where μ_s and $\Delta\mu$ set the value of the coefficient friction in the static and the highly dynamical limits. Two questions arise naturally from the comparison between discrete and continuum granular simulations. The first question is: Is the dependence of the friction μ
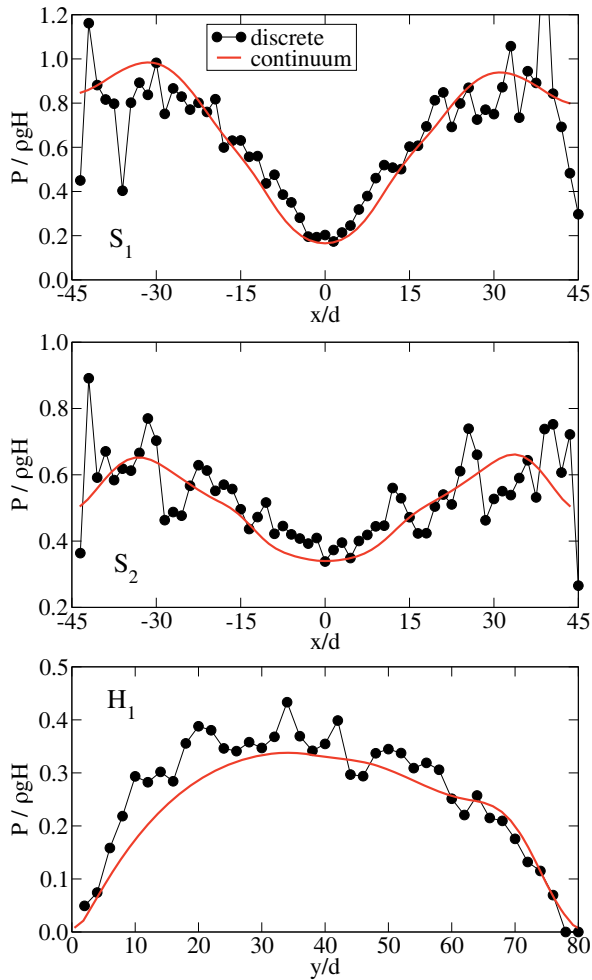
Fig. 9. Profile of the pressure P (normalized by $\rho g H$) along the horizontal cross-sections S_1 and S_2 and vertical axis H_1 (at time $T = 10\sqrt{gd}$), for the continuum (plain line) and the discrete (● symbols) simulations of granular silos with $L = 11.2d$. (See fig. 1 for localization of S_1, S_2 and H_1.)

on the inertial number I a crucial ingredient for reproducing the granular phenomenology? The second question is: Is it possible to tune efficiently the different parameters to increase quantitatively the agreement? Answering these points may moreover shed some light on the physical meaning of the parameters C and k of the continuum Beverloo scaling $Q = C\sqrt{g}(L - kd)^{3/2}$. To this point, the effect of the numerical grid over which the continuum flow is solved is also evaluated.

6.1 Tuning the rheological parameters

It is clear that the yield stress properties of the material have a strong effect on the pressure field around the outlet, where both the friction and the shear rate may rapidly vary [11]. This is illustrated in fig. 10 where the pressure profiles along the cross-sections S_1 and S_2 and along the horizontal axis H_1 are plotted for a continuum discharge using different values of the rheological parameters μ_s and

$\Delta\mu$. Increasing the static friction μ_s decreases the pressure in the bulk and close to the outlet, thereby decreasing local pressure gradients (hence affecting discharge velocity). Increasing the dependence on the inertial number —namely increasing $\Delta\mu$ for a given μ_s— allows to decrease the pressure only in the areas of higher shear, namely in the area of the outlet. As we will see in the following, this difference is of importance in the perspective of adjusting parameters to achieve quantitative agreement between continuum and discrete granular systems.

In a first series of continuum simulations, we set the parameter $\Delta\mu$ to zero: the dependence on the inertial number is suppressed. The static coefficient of friction μ_s only is considered and varied: $\mu_s = 0.3, 0.4, 0.5, 0.6, 0.7$ and 0.8. For each of these values, the corresponding continuum discharge is shown in fig. 11 for an outlet size $L = 14.1d$. We observe that for moderate values of μ_s, the discharge retains its linear shape, with a discharge rate diminishing with increasing μ_s. However, for larger values of μ_s, the discharge loses its linear quality: the flow rate is no longer constant. In other words, very large values of the static friction induce a departure from the phenomenology observed by Beverloo. This would certainly need precise characterization; in any case, the agreement with the granular silo behavior is lost.

In a second set of simulations, we restore the dependence on the inertial number by varying $\Delta\mu$, alternatively set to $0.3, 0.6, 0.9, 1.2$ and 1.5, while μ_s is kept to a fixed value 0.3. The corresponding discharges are shown in fig. 12. While the linearity is slightly compromised for $\Delta\mu = 1.5$, we observe that tuning $\Delta\mu$ is more efficient at slowing down the discharge rate than tuning μ_s, and preserves the constant discharge rate phenomenology. Hence, it appears that the dependence on the inertial number I, by including the shear-thickening properties of granular flows, allows for a more reliable description of the discrete granular behavior than a constant friction model does.

The influence of the value of both μ_s and $\Delta\mu$ on the parameters of the Beverloo scaling $Q = C\sqrt{g}(L-kd)^{3/2}$ is systematically analyzed in fig. 13, using either a constant friction model ($\Delta\mu = 0$), or the $\mu(I)$ flow law ($\Delta\mu \neq 0$). We observe that increasing the friction properties slows down the flow and reduces the effective outlet size, and that tuning the dynamical friction, that is, using the I-dependence, allows for a larger amplitude of variations for the Beverloo scaling, as already stressed. Note however that in both cases ($\Delta\mu = 0$ or $\Delta\mu \neq 0$), a Beverloo dependence is obtained: as discussed in [11], a frictional rheology without I dependence is enough to recover the Beverloo scaling.

One may question the legitimacy of using large values of the coefficient of friction (between 0.6 and 0.9) in continuum models, while effective friction measured in granular systems is rarely beyond 0.5 [17]. In [21] for instance, quantitative agreement was achieved in the case of the collapse of granular columns using the same set of numerical parameters as applied here for both continuum ($\mu_s = 0.32$, $\Delta\mu = 0.28$ and $I_0 = 0.4$), and discrete ($\mu_c = 0.5$, $e = 0.5$) simulations. The failure to obtain quantitative agreement
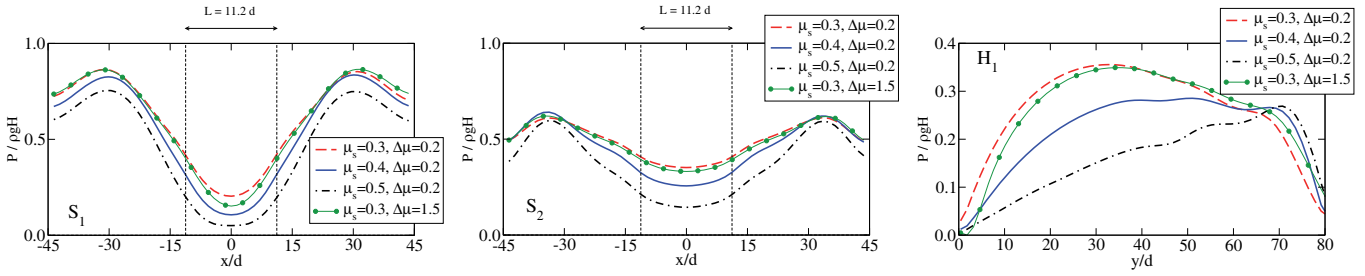
Fig. 10. Pressure profiles along the cross-sections S_1, S_2 and H_1 for identical continuum silos simulated with different values of the rheological parameters μ_s and $\Delta\mu$ (outlet size $L = 11.2d$).
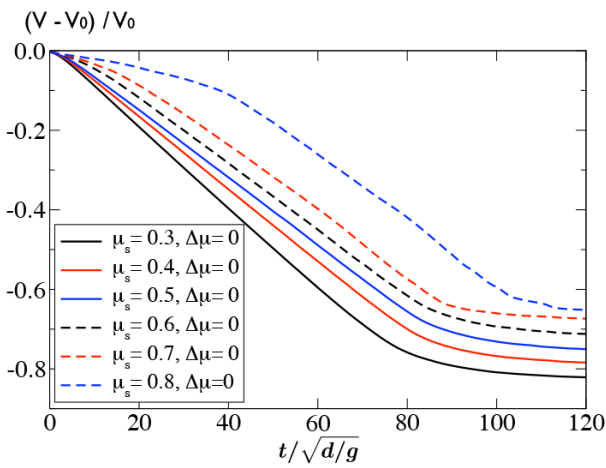

Fig. 11. (Color online) Normalized volume of matter left in the silo as a function of the normalized time $t/\sqrt{d/g}$ for continuum simulations with different values of the static coefficient of friction $\mu_s = 0.3$, 0.4, 0.5, 0.6, 0.7 and 0.8, with $\Delta\mu = 0$. ($L = 14.1d$).
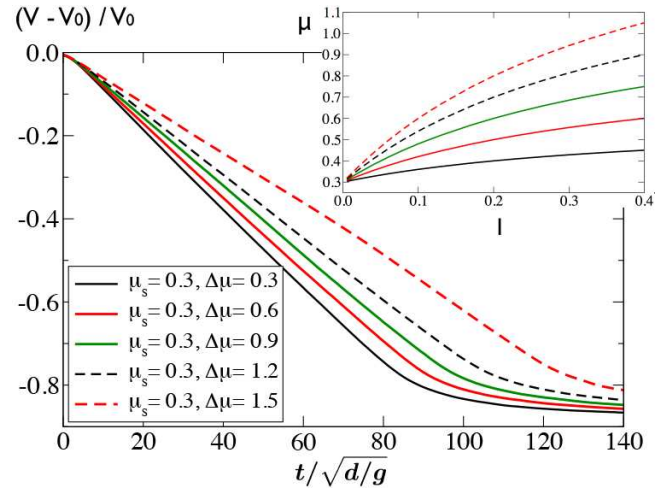

Fig. 12. (Color online) Normalized volume of matter left in the silo as a function of the normalized time $t/\sqrt{d/g}$ for continuum simulations with $\mu_s = 0.3$ and different values of $\Delta\mu = 0.3$, 0.6, 0.9, 1.2 and 1.5 ($L = 14.1d$). The inset graph shows the corresponding $\mu(I)$ dependence.

in the case of the silo for the same set of parameters suggests a possible dependence of the rheological properties on the geometrical flow configuration.

6.2 The influence of the numerical grid

So far, little was said about the influence of the size of the numerical cells over which the Navier-Stokes equation is solved in space in the continuum case. The Gerris flow solver uses an adaptive mesh refinement, which allows to adapt dynamically the resolution to the features of the flow. For the continuum simulations discussed so far, the width W is divided in 64 computation cells in the bulk, refined to 256 at the bottom, so that the outlet size is defined using 16 to 72 computation cells (see illustration in fig. 1). The size Δx of the numerical cells necessarily impacts on the spatial variations of shear rate and pressure and thus will reflect, to a certain extent, in the viscous properties of the granular flow. This may in turn affect the system mean's behavior, for instance the discharge rate and the corresponding Beverloo scaling. To quantify this effect, we perform a series of simulations with varying Δx, corresponding to 32, 64, 128 and 256 computation cells in

the bulk, respectively refined to 64, 128, 256 and 512 at the bottom of the silo. For each of these meshes, the flow rate is measured for outlet sizes between $L = 5d$ and $L = 22d$, as reported in fig. 14. We observe that Δx implies only marginal variations from a single Beverloo dependence. The effect of the numerical parameter Δx remains weak compared to the effect of the physical parameters μ_s, $\Delta\mu$ and L.

7 Influence of the boundary conditions

The boundary condition at the walls in all continuum simulations presented so far are no-slip boundary conditions. Although convenient, this may contradict the observation of slip velocities at rigid walls in a variety of experimental settings. In [52], discrete simulation shows that the slip velocity for dense granular flows obeys a Navier condition, with a dependence on the friction properties of the contacts. Without entering this degree of description at this stage, one may nevertheless speculate whether a free-slip velocity condition is more suited than a no-slip condition, and whether this change of boundary conditions would significantly affect the flow.
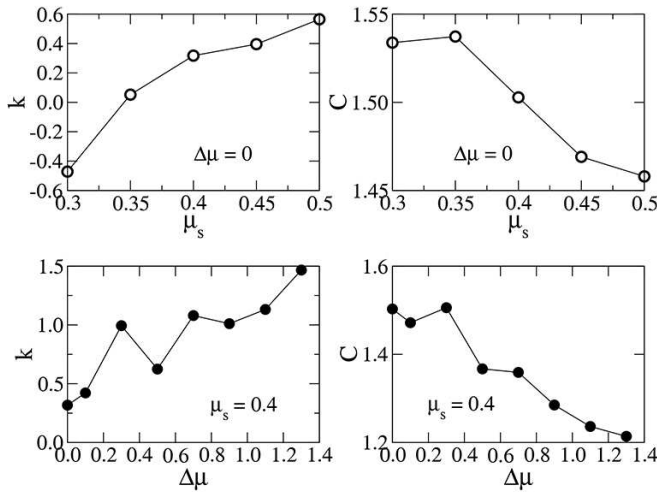
Fig. 13. Parameters k and C of the Beverloo scaling $\bar{Q} = C(\bar{L} - k)^{3/2}$ as a function of the friction parameters μ_s and $\Delta\mu$ of the $\mu(I)$ flow law $\mu = \mu_s + \Delta\mu/(1 + I_0/I)$.

Fig. 14. The Beverloo dependence for a continuum silo discharge simulated with different mesh refinement.

To clarify this aspect, we perform a continuum discharge with a free-slip condition for the velocity at both side walls, and compare it with the case of a no-slip condition. The volume left in the silo as a function of time for both cases is shown in fig. 15: the two evolutions are virtually indistinguishable. In the course of the discharge, velocity profiles remain essentially identical (not shown); this can be explained by the fact that velocities at the walls are zero in silo settings, hence not affected by slip/no-slip conditions. Pressure profiles show marginal differences only. At the onset of the discharge, the no-slip condition induces a lower pressure at the walls closer to the bottom than the free-slip condition does. This effect endures until the end of the discharge, although in a lesser extent; yet it has no consequence on the pressure field in the vicinity of the outlet and in the flow area. More interestingly, the difference of boundary conditions affects the shape of the free surface close to the walls all through the discharge: the no-slip condition induces a convex tail of material adhering to the walls, when the free-slip condition has a nearly flat free surface in this area, more in accordance to the observation of granular systems. Far from the walls however, the shape of the free surface is identical for both boundary conditions.

We can thus conclude that the boundary conditions at the walls do not affect the essential features of the continuum silo discharge. This is expected since the flow characteristics in a silo are dictated by the local condition created by the outlet, while velocities are small or zero far from that region. It appears that the silo configuration is poorly suited to address in detail the relevance of free-slip, no-slip or mixed conditions at walls, and that other flow geometries would certainly give more information on the influence of boundary conditions when simulating continuum granular flows.
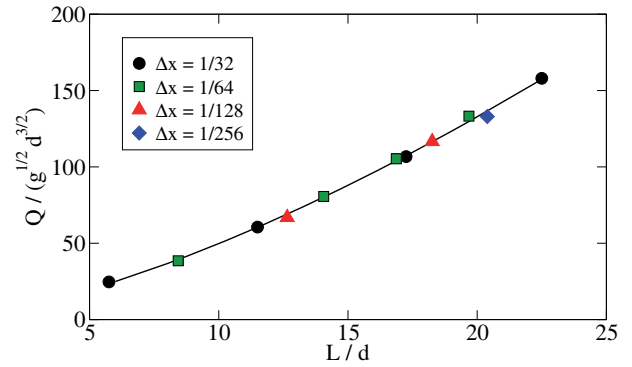
8 Conclusion

Applying a continuum Navier-Stokes solver with the $\mu(I)$ flow law implemented to model the viscous behavior of dense granular flows, we simulate the discharge of the granular silo from the early stages of the discharge until complete release of the material. Discrete simulations of the same system using the Contact Dynamics algorithm are performed to allow for systematic comparison between the two approaches. Discharge rate, velocity field and pressure field are addressed. In a first step, we do not attempt to adjust the rheological parameters to achieve quantitative agreement between continuum and discrete discharge rates, but focus on qualitative aspects. Analyzing the shape of the velocity field at different locations in the flow, we find that continuum and discrete approaches show a good qualitative agreement in the areas of rapid flow, but tend to differ in the area of slow shear, namely near the outlet edges or in the bulk: the transition from a flowing state to a static one seems sharper in the continuum model. Focusing on the shape of the pressure profiles, the agreement also appears fairly good. Discrete and continuum simulations share the following features: a marked dip of pressure above the outlet, the existence of two high-pressure regions on one and the other side of the outlet, and a slight decrease close to the walls. The Beverloo scaling is recovered for both discrete and continuum systems. The influence of the rheological parameters of the $\mu(I)$ flow law on the parameters of the Beverloo scaling is systematically investigated, while the effect of the numerical resolution mesh is also quantified and found to be weak.

Adjusting the rheological parameters of the continuum model to match quantitatively the discrete behavior reveals however some potential problems. While the dependence on the inertial number, which is the key ingredient of the friction law implemented in the continuum model, is found to increase the ability of the latter to mimic discrete flows, the values of the continuum friction parameters needed to achieve quantitative correspondence between the two approaches are larger than the typical values measured in granular flows. In [21], quantitative agreement was achieved in the case of the collapse of granular columns using the set of numerical parameters
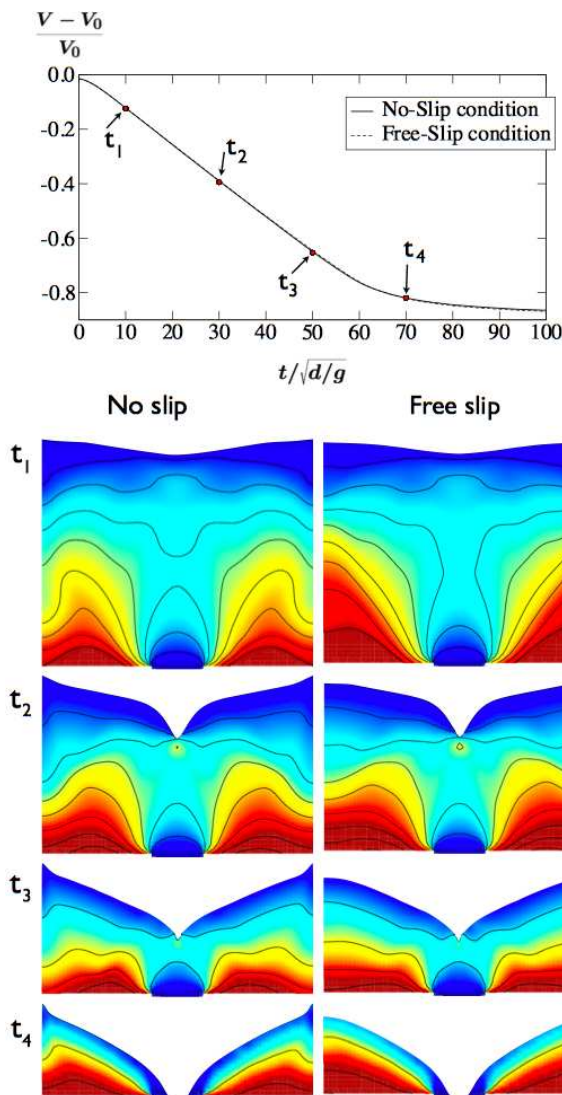
Fig. 15. (Color online) Top graph: discharge of the continuum silo ($L = 14.1$) in the course of time for a no-slip condition and a free-slip condition at walls. Snapshots: map of the pressure at different instants t_1, t_2, t_3 and t_4 for no-slip (left) and free-slip (right) conditions.

applied here for continuum and discrete simulations. The failure to obtain quantitative agreement in the case of the silo for the same set of parameters suggests a possible dependence of the flow properties on the geometrical flow configuration. Such known dependences include the width and height of a confined chute flow for instance [53,54]. Likewise, the effect of the size of the silo would deserve further investigation, particularly in the case of small systems [55]. The existence of "non-local" effects, causing the friction to depend on the state of the system elsewhere rather than being a purely local property, may also possibly account for the discrepancy between continuum and discrete simulations [26]. Their recent implementation in the case of steady flows leads to improved agreement between discrete and continuum granular systems, and allow for including systems size effects [27,55]. They are thus ex-

pected to allow for an improvement of the performances of the continuum model in the case of the silo configuration, specifically in areas of slow shear, and form a likely perspective of this work. At this stage however, we may conclude that the general ability of the continuum $\mu(I)$ flow law to reproduce the main features of the discharge of a granular silo is very encouraging.

References

1. T. Le Pennec, K.J. Måløy, E.G. Flekkøy, J.C. Messager, M. Ammi, Phys. Fluids **10**, 3072 (1998).
2. A. Janda, R. Harich, I. Zuriguel, D. Maza, P. Cixous, A. Garcimartín, Phys. Rev. E **79**, 031302 (2009).
3. D.M. Walker, Chem. Engng. Sci. **21**, 975 (1966).
4. C.E. Davies, V. Chew, New Zealand J. Dairy Sci. Techol. **18**, 47 (1983)..
5. W.A. Beverloo, H.A. Leniger, J. van de Velde, Chem. Eng. Sci. **15**, 260 (1961).
6. X.L. Wu, K.J. Maløy, A. Hansen, M. Ammi, D. Bideau, Phys. Rev. Lett. **71**, 1363 (1993).
7. J.M.N.T. Gray, K. Hutter, Contin. Mech. Thermodyn. **9**, 341 (1997).
8. A. Samadani, L. Mahadevan, A. Kudrolli, J. Fluid Mech. **452**, 293 (2002).
9. J.M. Rotter, J.M.F.G. Holst, J.Y. Ooi, A. M. Sanad, Philos. Trans. R. Soc. London, Ser. A **356**, 2685 (1998).
10. K. Kamrin, Int. J. Plasticity **26**, 167 (2010).
11. L. Staron, P.-Y. Lagrée, S. Popinet, Phys. Fluids **24**, 113303 (2012).
12. J. Sun, S. Sundaresan, arXiv:1207.1751v1 [cond-mat.soft] (2012).
13. C. Mankoc, A. Janda, R. Arévalo, J.M. Pastor, I. Zuriguel, A. Garcimartín, D. Maza, Granular Matter **7**, 407 (2007).
14. C.H. Rycroft, K. Kamrin, M.Z. Bazant, J. Mech. Phys. Solids **57**, 828 (2009).
15. P. Claudin, J.-P. Bouchaud, M.E. Cates, J.P. Wittmer, Phys. Rev. E **57**, 4441 (1998).
16. J.-N. Roux, Phys. Rev. E **61**, 6802 (2000).
17. GDR MiDi, Eur. Phys. J. E **14**, 341 (2004).
18. F. da Cruz, S. Emam, M. Prochnow, J.-N. Roux, F. Chevoir, Phys. Rev. E **72**, 021309 (2005).
19. P. Jop, Y. Forterre, O. Pouliquen, Nature **441**, 727 (2006).
20. G.B. Crosta, S. Imposimato, D. Roddeman, J. Geophys. Res. **114**, F03020 (2009).
21. P.-Y. Lagrée, L. Staron, S. Popinet, J. Fluid Mech. **686**, 378 (2011).
22. L. Lacaze, R.R. Kerswell, Phys. Rev. Lett. **102**, 108305 (2009).
23. J. Chauchat, M. Médale, Comput. Methods Appl. Mech. Engrg. **199**, 439 (2010).
24. C. Ancey, P. Coussot, P. Evesque, J. Rheol. **43**, 1673 (1999).
25. T.J. Hatano, Phys. Rev. E **75**, 060301 (2007).
26. O. Pouliquen, Y. Forterre, Philos. Trans. R. Soc. A **367**, 5091 (2009).
27. K. Kamrin, G. Koval, Phys. Rev. Lett. **108**, 178301 (2012).
28. J. Sun, S. Sundaresan, J. Fluid Mech. **682**, 590 (2011).

29. S. Popinet, J. Comput. Phys. **190**, 572 (2003).
30. S. Popinet, J. Comput. Phys. **228**, 5838(2009 (.)
31. M. Jean, J.-J. Moreau, *Unilaterality and dry friction in the dynamics of rigid bodies collection*, in *Proceedings of the Contact Mechanics International Symposium*, edited by A. Curnier (Presses Polytechniques et Universitaires Romandes, 1992) pp. 31-48.
32. F. Radjai, V. Richefeu, Mech. Mater. **41**, 715 (2009).
33. F. Radjai, L. Brendel, S. Roux, Phys. Rev. E **54**, 861 (1996).
34. I. Zuriguel, A. Garcimartín, D. Maza, L.A. Pugnaloni, J.M. Pastor, Phys. Rev. E **71**, 051303 (2005).
35. A. Janda, I. Zuriguel, D. Maza, Phys. Rev. Lett. **108**, 248001 (2013).
36. A.V. Potapov, C.S. Campbell, Phys. Fluids **8**, 2884 (1996).
37. J. Choi, A. Kudrolli, M.Z. Bazant, J. Phys: Condens. Matter, **17**, S2533 (2005).
38. I. Bartos, I.M. Jánosi, Granular Matter **9**, 81 (2006).
39. H.G. Sheldon, D.J. Durian, Granular Matter **12**, 579 (2010).
40. M.A. Aguirre, J.G. Grande, A. Calvo, L.A. Pugnaloni, J.-C. Géminard, Phys. Rev. E **83**, 061305 (2011).
41. C. González-Montellano, F. Ayuga, J.Y. Ooi, Granular Matter **13**, 149 (2011).
42. J.E. Hilton, P.W. Cleary, Phys. Rev. E **84**, 011307 (2011).
43. H.A. Janssen, Zeitschr. Vereines Deutsch. Ing. **39**, 1045 (1895).
44. M. Sperl, Granular Matter **8**, 59 (2006).
45. G. Ovarlez, C. Fond, E. Clément, Phys. Rev. E **67**, 060302 (2003).
46. C. Perge, M.A. Aguirre, P.A. Gago, L.A. Pugnaloni, D. Le Tourneau, J.-C. Géminard, Phys. Rev. E **85**, 021303 (2012).
47. R.M. Nedderman, *Static and Kinematics of Granular Materials* (Cambridge University Press, 1992).
48. D. Hirshfeld, Y. Radzyner, D.C. Rapaport, Phys. Rev. E **56**, 4404 (1997).
49. P.A. Langston, U. Tüzün, D.M. Heyes, Chem. Engin. Sci. **50**, 967 (1995).
50. M.F. Djouwe Meffeja, PhD Thesis, Université de Rennes 1 (2012).
51. A. Garcimartín, I. Zuriguel, A. Janda, D. Maza, Phys. Rev. E **84**, 031309 (2011).
52. R. Artoni, A.C. Santomaso, M. Go, P. Canu, Phys. Rev. Lett. **108**, 238002 (2012).
53. P. Jop, Y. Forterre, O. Pouliquen, J. Fluid Mech. **541**, 167 (2005).
54. O. Pouliquen, Phys. Fluids **11**, 542 (1999).
55. D.L. Henann, K. Kamrin, Proc. Natl. Acad. Sci. U.S.A. **110**, 6730 (2013).